JACS
JOURNAL OF THE AMERICAN CHEMICAL SOCIETY
pubs.acs.org/JACS
Article

Distance-Selected Topochemical Dehydro-Diels–Alder Reaction of 1,4-Diphenylbutadiyne toward Crystalline Graphitic Nanoribbons

Peijie Zhang, Xingyu Tang, Yida Wang, Xuan Wang, Dexiang Gao, Yapei Li, Haiyan Zheng, Yajie Wang, Xinxin Wang, Riqiang Fu, Mingxue Tang, Kazutaka Ikeda, Ping Miao, Takanori Hattori, Asami Sano-Furukawa, Christopher A. Tulk, Jamie J. Molaison, Xiao Dong, Kuo Li,* Jing Ju,* and Ho-kwang Mao

Cite This: https://dx.doi.org/10.1021/jacs.0c08274

ABSTRACT: Solid-state topochemical polymerization (SSTP) is a promising method to construct functional crystalline polymeric materials, but in contrast to various reactions that happen in solution, only very limited types of SSTP reactions are reported. Diels–Alder (DA) and dehydro-DA (DDA) reactions are textbook reactions for preparing six-membered rings in solution but are scarcely seen in solid-state synthesis. Here, using multiple cutting-edge techniques, we demonstrate that the solid 1,4-diphenylbutadiyne (DPB) undergoes a DDA reaction under 10–20 GPa with the phenyl as the dienophile. The crystal structure at the critical pressure shows that this reaction is "distance-selected". The distance of 3.2 Å between the phenyl and the phenylethynyl facilitates the DDA reaction, while the distances for other DDA and 1,4-addition reactions are too large to allow the bonding. The obtained products are crystalline armchair graphitic nanoribbons, and hence our studies open a new route to construct the crystalline carbon materials with atomic-scale control.

INTRODUCTION

The mechanical, electrical, optical, and chemical properties of the polymeric carbon material highly depend on the ordering of their local and long-range structure. One promising approach to obtain crystalline polymeric structures is solid-state topochemical polymerization (SSTP). The unsaturated molecules are confined in crystal lattices and usually react with a minimum movement; hence, the structure of the product can be predicted and designed from that of the reactant crystal via a crystal-to-crystal route.[1−5] The most well-known example is the 1,4-addition polymerization of diacetylenes, which yields conjugated linear en-yne crystals with excellent optical and electrical properties.[5−11] Unfortunately, the reaction types of the SSTP are very limited, and only a few monomers like diacetylene,[5−11] triacetylene,[12] diene,[13] triene,[14] and olefins[15] can polymerize topochemically through the 1,4-addition or [2 + 2] cycloaddition reaction. New SSTP reactions are still needed to be developed.

Diels–Alder (DA) reactions are textbook cyclization reactions between diene and ethene and are widely used for building a new six-membered carbocycle. Recently, dehydro-Diels–Alder (DDA) reactions have been reported extensively, where at least one of the double bonds is replaced by a triple bond. This reaction is recognized as an ideal method for synthesis of the arene and the sp^2 carbon materials.[16−22] However, both DA and DDA reactions are scarcely seen in solid-state reactions because arranging the diene and dienophile in an appropriate geometric configuration in a solid is very challenging.[4] Applying high pressure is proven to be an effective way to regulate molecular stacking, compress the intermolecular distance, and thus induce the topochemical reaction in a constrained crystallized environment.[23−27] For example, acetylene molecules freeze in an orthorhombic lattice under high pressure and polymerize to *cis*-polyacetylene instead of the *trans*-isomer through a topochemical route.[28] Very recently, 1,4-diphenylbutadiyne (DPB) was reported to polymerize under high pressure.[29] In this work, we investigated the high-pressure SSTP of DPB and found that the reaction starts via an unexpected DDA reaction with phenyl as the dienophile instead of a 1,4-addition reaction between diynes. The geometric configuration of the molecules before the reaction and the structure of the produced graphitic nanoribbon are discussed. From this we concluded the distance-selectivity between DDA and the 1,4-addition reaction in this crystal, and a DDA reaction is hence added into the toolbox of SSTP.

Received: August 1, 2020
Published: September 8, 2020

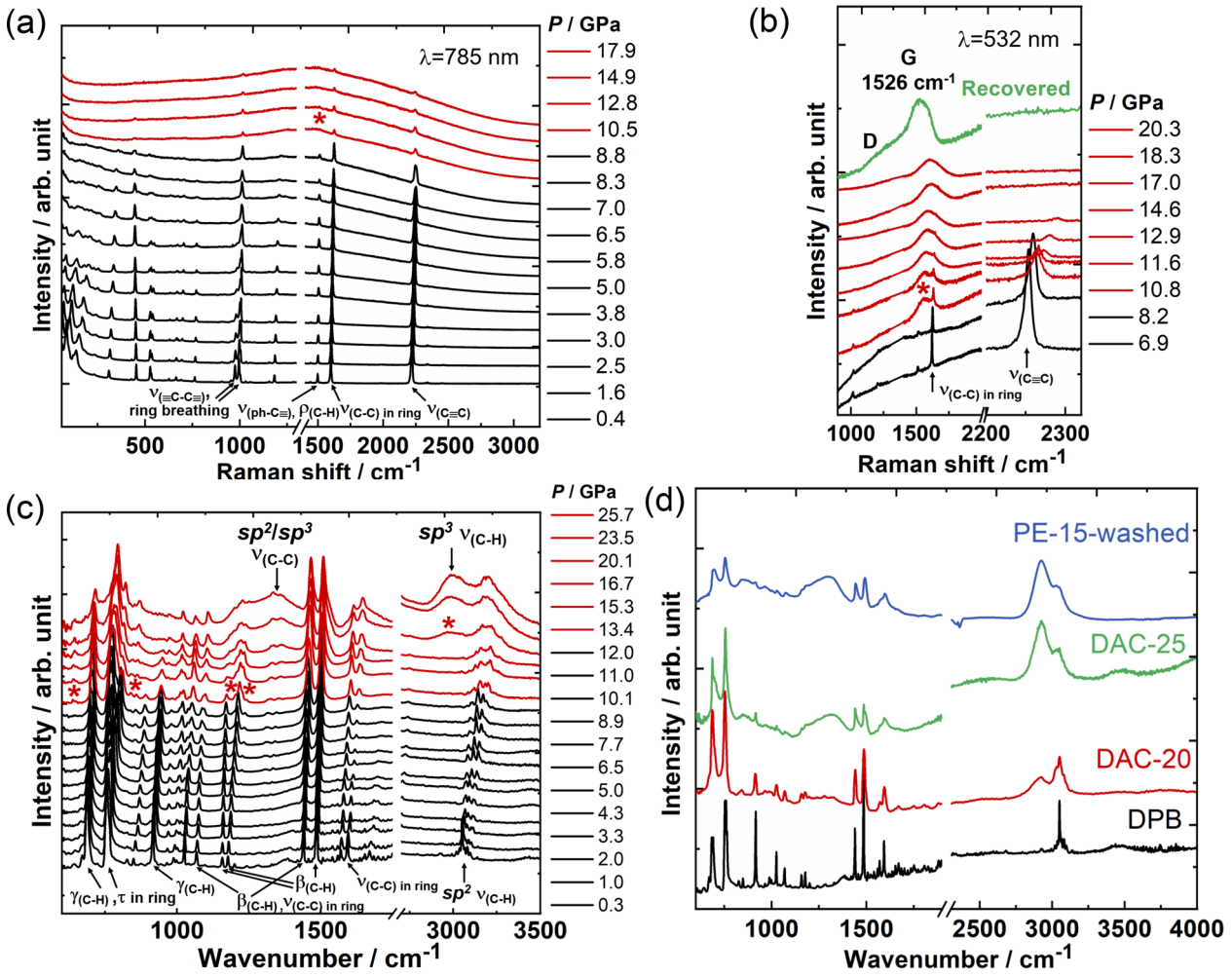

Figure 1. (a, b) In situ high-pressure Raman spectra of DPB measured by the lasers with wavelengths of 785 and 532 nm, respectively. Recovered represents the sample decompressed from 20.3 GPa to ambient pressure. (c) In situ high-pressure IR spectra of DPB. (d) IR spectra of DPB under 0.3 GPa and samples recovered from different pressures. DAC-20 and DAC-25 stand for the samples recovered from 20 and 25 GPa, respectively, in a diamond anvil cell (DAC). PE-15-washed is the pure product, obtained by the sample synthesized by Paris–Edinburgh (PE) Press at 15 GPa and washed with dichloromethane (CH_2Cl_2) to remove any unreacted DPB. The asterisks stand for the appearance of new peaks. ν represents the stretching vibration, ρ represents the rocking vibration, γ stands for the out-of-plane bending vibration, τ stands for the torsion vibration, and β stands for the in-plane bending vibration.

RESULTS AND DISCUSSION

Raman and IR Spectra that Reveal Pressure-Induced Polymerization between Phenyl and Acetylene Groups. DPB (purity confirmed by X-ray diffraction as shown in Figure S1) was compressed in diamond anvil cells (DACs) up to 25 GPa. In situ Raman spectra of DPB were measured using lasers with wavelengths of 785 (Figure 1a) and 532 nm (Figure 1b), respectively. As shown in Figure 1a, the Raman spectra maintain their profile below 10 GPa. All of the peaks blue shift gradually, and no new peaks are observed. This excludes the reported 1,4-addition reaction below 10 GPa,[29] which would result in a new triple bond with its stretching mode at 2100 cm^{-1}, and the obvious weakening of the C≡C stretching ($\nu_{(C\equiv C)}$) mode of monomers.[30] Above 10 GPa, all of the Raman peaks of DPB are notably weakened and a new broad band appears, which is more obvious around 1550 cm^{-1} using a 532 nm excitation (Figure 1b). This band shifts to 1526 cm^{-1} when decompressed to ambient pressure, and another broad band at 1250 cm^{-1} is also observed. These two bands are attributed to the D-band and G-band of the carbon materials, which suggests that the obtained black products (pressure-induced polymerization (PIP)-DPB) have a graphitic structure. In situ IR spectra were also measured as shown in Figure 1c. Below 13.4 GPa, the IR spectra keep their profile and the peaks smoothly blue-shift (Figure S2), which suggests that no phase transition or reaction of DPB occurs below 10 GPa. Above 13.4 GPa, several new peaks at 638, 837, 1203, and 1228 cm^{-1} are observed, and the intensities of the peaks centered at 890 and 946 cm^{-1} decrease. Meanwhile, the intensities of two broad peaks at 1321 and 1357 cm^{-1} start to increase. All of these indicate the beginning of the reaction. At 20.1 GPa, a new peak was observed at 2978 cm^{-1}, and its intensity was enhanced significantly with increasing pressure. This is unambiguously attributed to the $\nu_{(C-H)}$ mode of sp^3 carbon, which demonstrates the addition reaction of phenyls. By comparing the IR spectra of the recovered samples decompressing from different pressures with the pure product obtained by removing the reactant (PE-15-washed, Figure 1d), we confirmed that DPB reacts completely around 25 GPa.

Crystal Structure at Threshold Pressure. In situ synchrotron X-ray diffraction (XRD) shows that DPB

https://dx.doi.org/10.1021/jacs.0c08274
J. Am. Chem. Soc. XXXX, XXX, XXX−XXX

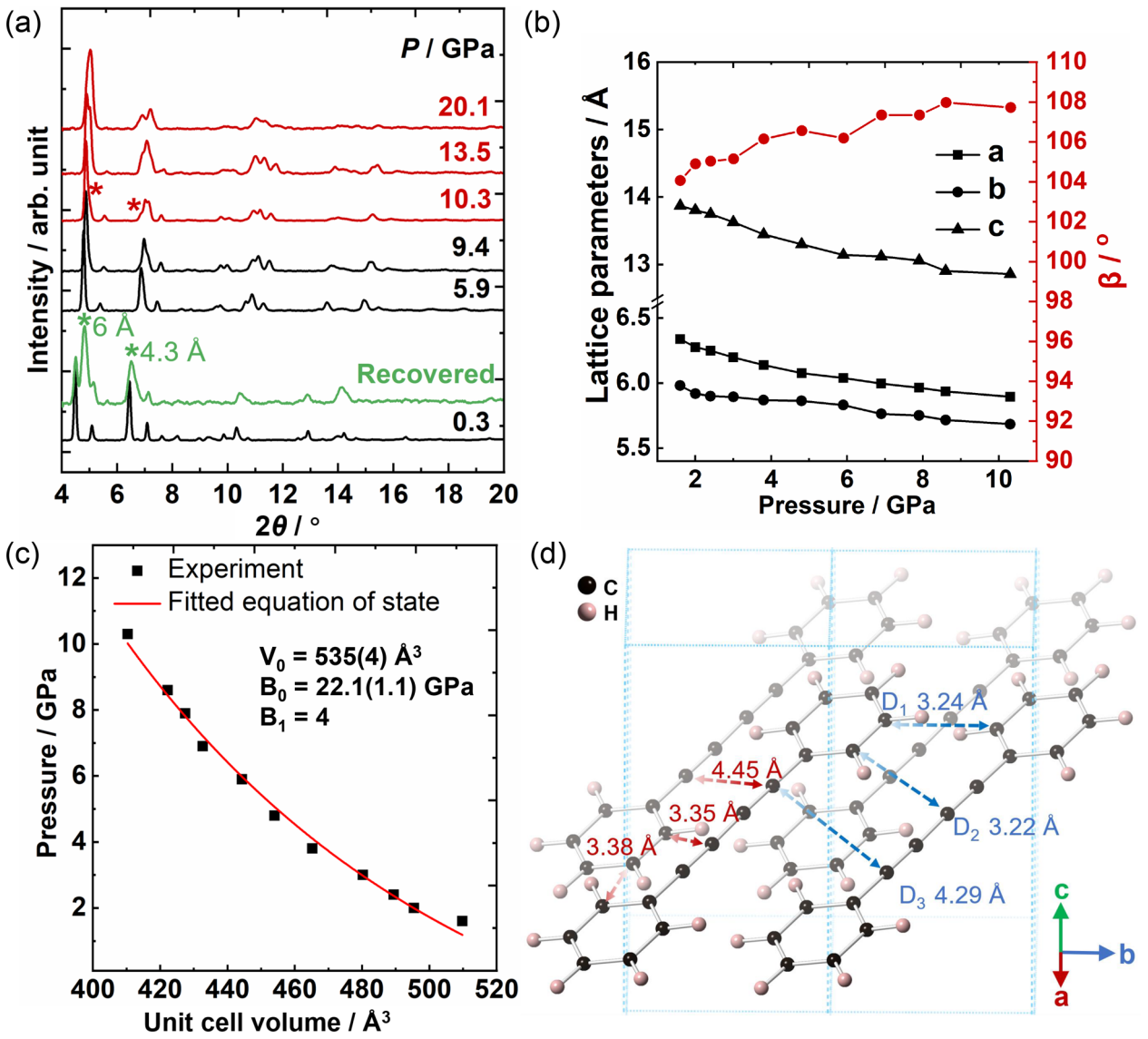

Figure 2. (a) Selected in situ X-ray diffraction patterns of DPB under applied pressure, including that recovered from 20.1 GPa. The peaks from the PIP-DPB are marked by the asterisks. (b) Evolution of corresponding lattice parameters of DPB in the range from 1.6 to 10.3 GPa. The error bar of the lattice parameters is less than the symbol size. (c) Unit cell volume of DPB as a function of pressure. (d) Crystal structure of DPB optimized by density functional theory (DFT) calculation based on the experimental lattice under 10 GPa.

maintains the monoclinic phase from ambient pressure ($P2_1/n$, a = 6.57 Å, b = 6.02 Å, c = 14.51 Å, β = 102.38°) to 10 GPa (Figures 2a and S3). The corresponding lattice parameters were obtained by Rietveld refinement (Figure 2b). The $P-V$ relationship of DPB was then fitted by one 3rd-order Birch–Murnaghan equation of state[31] with V_0 = 535(4) Å^3, B_0 = 22.1 (1.1) GPa, and B_1 = 4 (Figure 2c). This also suggests that no phase transition or reaction of DPB occurs below 10 GPa, in agreement with the IR and Raman data. Above 10 GPa, new diffraction peaks appear at 5.9 and 4.1 Å that are attributed to PIP-DPB (Figure 2a). In situ neutron diffraction data of the deuterated DPB were also collected because of its high sensitivity to carbon and hydrogen (deuterium). Several new diffraction peaks are observed from 2.5 to 3.5 Å above 10 GPa, which are also ascribed to the PIP-DPB (arrows in Figure S4).

The crystal structure of DPB at the threshold pressure (10 GPa) was then determined by Rietveld refinement and subsequently optimized by density functional theory (DFT) calculation with the lattice parameters fixed at the experimental value. The corresponding Rietveld refinement plot (Figure S5), Rietveld refinement results (Table S1), and crystal structure CIF file are listed in the Supporting Information. As shown in Figure 2d, the stackings of molecules along the a and b axes are similar at 10 GPa, and the intermolecular C···C distances ($d_{C\cdots C}$) along the b axis are slightly smaller. The nearest $d_{C\cdots C}$ are 3.24 Å (D_1) between the phenyl groups and 3.22 Å (D_2) between the alkynyl and phenyl group, respectively. In contrast, the separation of the 1,4′ carbon along the b axis is 4.29 Å (D_3), which is still greater than the required reaction distance for the SSTP of diynes (4 Å).[9,10] This implies that DPB is unable to react along the traditional 1,4-addition path but instead has a totally new reaction path containing phenyl and alkyne groups, which is consistent with our Raman and IR results.

Polymerization Product of DPB. To understand the structure of polymerized products, we synthesized samples by Paris–Edinburgh (PE) Press at 10 (PE-10), 15 (PE-15), and 20 GPa (PE-20), respectively. The colors of all the samples

https://dx.doi.org/10.1021/jacs.0c08274
J. Am. Chem. Soc. XXXX, XXX, XXX–XXX

underwent significant changes, from white (original DPB) to brown (PE-10) and brownish black (PE-15 and PE-20). PE-10 is soluble in dichloromethane (CH_2Cl_2), and its XRD and liquid-state nuclear magnetic resonance (NMR) spectrum shows that it is composed of DPB (Figures S6 and S7). Both PE-15 and PE-20 show new diffractions at 13.0 and 5.9 Å, which are attributed to the polymerized products (Figure 3a).

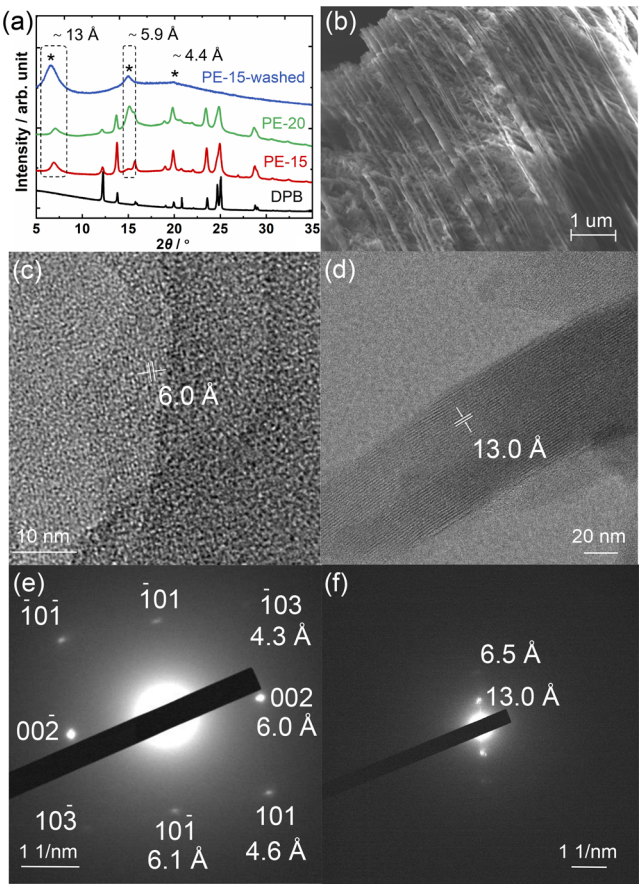

Figure 3. (a) Lab-XRD patterns of the recovered samples PE-15, PE-20, PE-15-washed, and original DPB at ambient pressure. The diffraction peaks ascribed to the product are marked by the asterisks. (b) SEM image of PE-15-washed. (c, e) High-resolution transmission electron microscope (HRTEM) image and electron diffraction of phase I with lattice parameters a = 6.15 Å, c = 13.10 Å, and β = 113°. (d, f) HRTEM image and electron diffraction of phase II.

The intensity of the peak at 5.9 Å is significantly enhanced for PE-20 compared to PE-15, indicating that there are probably two ordered phases represented by these two peaks, respectively. The sample PE-15 was washed with CH_2Cl_2 to remove any unreacted DPB (labeled PE-15-washed), and its XRD pattern only contains the peaks of the product at 13.0, 5.9, and 4.4 Å (marked by the asterisks in Figure 3a).

The scanning electron microscope (SEM) measurements show that PE-15-washed has ribbon structures (Figure 3b). From selected area electron diffraction (SAED) patterns under a high-resolution transmission electron microscope (HRTEM), two kinds of diffraction patterns featuring diffraction peaks at $d \approx$ 5.9 and 13.0 Å, respectively, were observed (Figure 3c–f), consistent with the results of XRD. These two patterns cannot be found simultaneously in one particle after many attempts, which indicates that two phases are present in PE-15-washed. For the first phase ($d \approx$ 5.9 Å, referred to as phase I), the SAED pattern in Figure 3e is indexed as a = 6.15 Å, c = 13.10 Å, and β = 113° with the Pn or higher symmetry space group, which is closely related to the DPB lattice. The hkl ($k \neq 0$) diffractions were not observed, even if the particles were tilted. This suggests that the periodicity along the b axis is destroyed and implies that the reaction occurs along the b axis in DPB. For phase II, on the basis of the HRTEM image (Figure 3d) and SAED pattern (Figure 3f), it is suggested to be a kind of nanoribbon structure with a width of 13 Å.[32]

The similarity between the lattice of phase I and that of DPB suggests that phase I is the direct polymerized product of DPB under applied pressure. As shown in Figure 2d, at the critical pressure the two smallest $d_{C\cdots C}$ (D_1 and D_2) of DPB are 3.24 and 3.22 Å, respectively. Considering that the similar critical distance of reaction for acetylene is 3.1 Å,[28] a DDA reaction with a bonding route through D_1 and D_2 is proposed (Scheme 1a). The geometry of this reaction is similar with that of the

Scheme 1. (a) Proposed DDA Reaction from DPB to GNR That Starts with Forming New C−C Bonds through D_1 and D_2, (b) Diagram of Hopf Cyclization, (c) Geometric Requirements of 1,4-Addition Topochemical Polymerization of Diynes in the Solid State, and (d) Other DDA Reaction Routes for Comparison

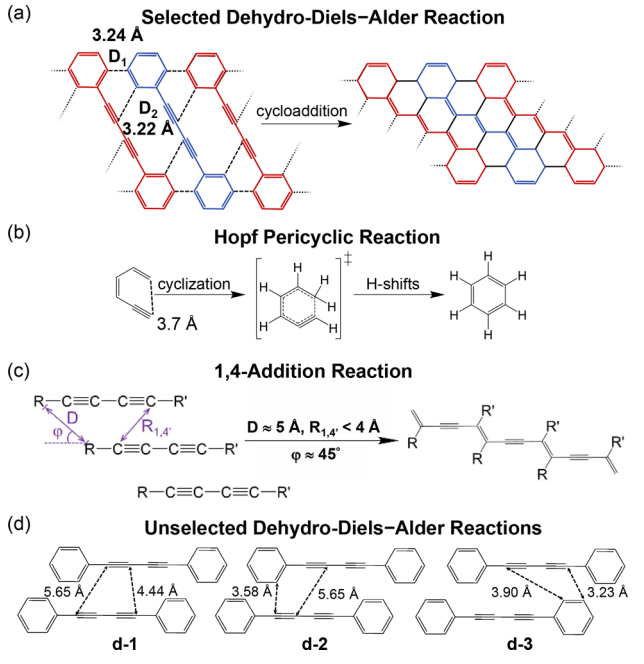

Hopf cyclization,[33] in which the hexa-1,3-dien-5-yne cyclizes with the distance between the two reactive carbon atoms (1,6) at 3.7 Å (Scheme 1b).[34] In our work, D_1 (3.24 Å) and D_2 (3.22 Å) in DPB are much smaller, which indicates a much higher possibility of reaction. On the basis of the proposed reaction route, we built the crystal structure of phase I and optimized it with the lattice parameters a, c, and β fixed at the SAED result. A monoclinic lattice with b = 4.2 Å was obtained, and the structure is shown in Figure 4a. The simulated SAED pattern is consistent with the experimental result (Figures 3e and S8), which confirms the proposed graphitic nanoribbon (GNR) model (referred to as GNR-1). In GNR-1, 5/8 of the carbon atoms are bonded to hydrogen atoms, including 2/8 sp^2-carbons on the edge and 3/8 sp^3-carbons next to the edge, and

https://dx.doi.org/10.1021/jacs.0c08274
J. Am. Chem. Soc. XXXX, XXX, XXX−XXX

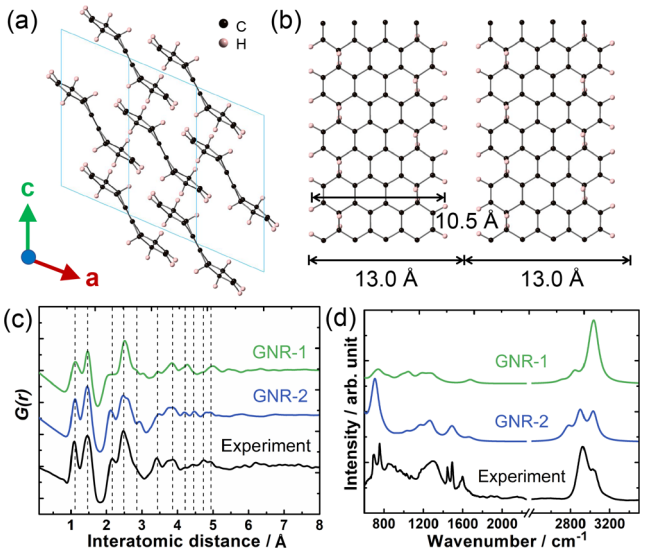

Figure 4. (a) Crystal structure of GNR-1 viewed along the *b* axis. (b) Structure of GNR-2 and its calculated width. (c) Neutron PDF experiment data of deuterated sample PE-15-washed and the simulated PDFs $G(r)$ of structural models GNR-1 and GNR-2. (d) IR spectra of PE-15-washed and calculated IR spectra of GNR-1 and GNR-2 at ambient pressure. Band shapes were modeled using a Lorentzian function with a full width at half-maximum (fwhm) of 100 cm^{-1}.[35]

the remaining 3/8 carbon atoms are sp^2-hybridized at the center of the ribbon. Inspired by this model, we proposed another GNR model (GNR-2) for phase II with higher conjugation by eliminating the hydrogen atoms inside the ribbon (Figure 4b). The distance from an edge hydrogen atom of GNR-2 to the opposite edge across the ribbon is ~10.5 Å. Considering the van der Waals radii of the hydrogen atoms (1.2 Å × 2), the total width of GNR-2 is ~13.0 Å, which is consistent with the value observed in the HRTEM and SAED experiments of phase II and, hence, supports the model.

The proposed structure models of GNR-1 and GNR-2 are further evidenced by the neutron pair distribution function (PDF), IR, and NMR. As shown in the PDF $G(r)$ plot in Figure 4c, the deuterated sample PE-15-washed has peaks at 1.45, 2.50, and 2.85 Å in the $G(r)$ plot, which are a clear feature of the graphitic structure (distance to the *o*-, *m*-, and *p*-carbons in a hexagonal ring). We simulated $G(r)$ patterns using these two GNR models, and they fit well with the experimental data (Figure 4c). We also simulated the IR spectra of GNR-1 and -2 using DFT, which also fit the experimental data very well (Figure 4d). The peaks centered at 694 and 755 cm^{-1} respond to the deformation of the carbon skeleton and out-of-plane vibration modes of C−H. The hump in the region of 1000−1400 cm^{-1} is recognized as in- or out-of-plane vibration modes of C−H, which also agrees with ref 32. The peaks at 1446 and 1492 cm^{-1} are the stretching vibration of sp^2 carbon at the center, while the bands at 1597 cm^{-1} are ascribed to the stretching mode of the sp^2 carbon at the edge. The C(sp^3)−H and C(sp^2)−H stretching modes can be identified by the peaks centered at about 2900 and 3000 cm^{-1}, respectively, indicating that a large number of hydrogen atoms appear on the GNR structure. The detailed assignments of the IR peaks are provided in Figures S9 and S10.

High-resolution ^{13}C cross-polarization (^1H−^{13}C) magic-angle-spinning (CPMAS) solid-state NMR of PE-15-washed were also measured to understand the local structure. In the PE-15-washed, the peaks of alkynyl carbons disappear compared to those at 77 and 82 ppm in DPB (Figure 5a). A

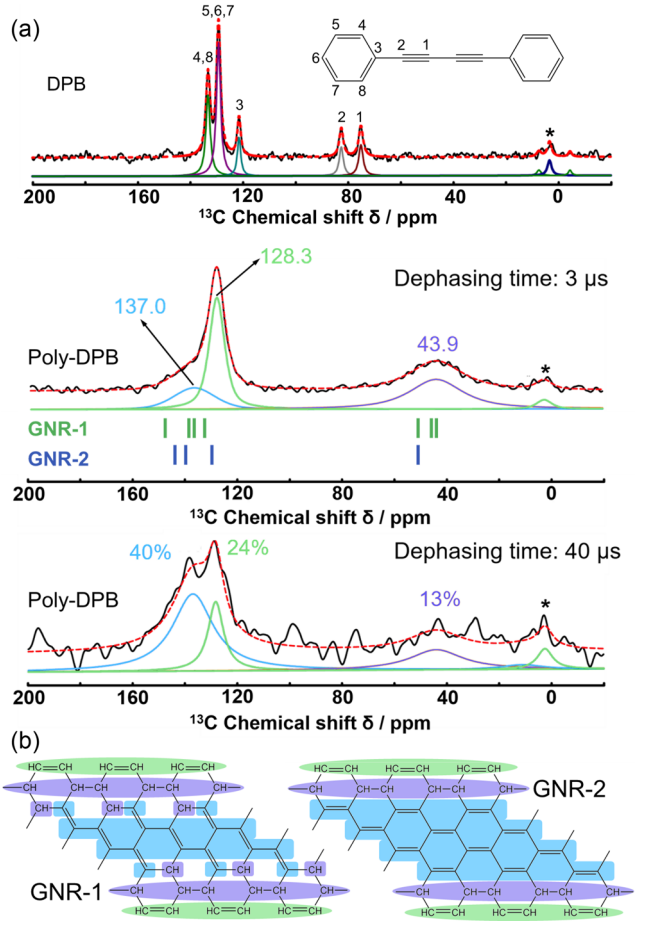

Figure 5. (a) ^{13}C CPMAS solid-state NMR spectra of DPB and PE-15-washed with different dephasing times (3 and 40 μs). The assignments of the peaks of DPB were given by the numbers marked in the DPB molecular structure. The black solid line and red dashed line represent the signal obtained from the experiment and its deconvolution result, respectively. The green and blue vertical lines represent the calculation NMR results of the GNR-1 and GNR-2 models, respectively. The percentages marked in the spectrum with a dephasing time of 40 μs are normalized to their respective signal intensities from the spectrum with a dephasing time of 3 μs. The asterisks indicate spinning side bands raised from the peaks in the range of 120−150 ppm. (b) Structure models of GNR-1 and GNR-2. The assignments of the isotropic peaks are donated and marked with corresponding colors to guide the eye.

new peak at ~43.9 ppm and an asymmetric broad peak at 120−150 ppm were observed. The latter can be fitted by two peaks at 128.3 and 137.0 ppm. The experimental results are consistent with the simulated NMR results (vertical lines in Figure 5a) based on the GNR-1 and GNR-2 models, which again confirms our proposed product models. When the dephasing time was prolonged from 3 to 40 μs, the peaks at 43.9 and 128.3 ppm weaken more quickly than that at 137 ppm, which means they are from the newly formed sp^3-C(−H) and sp^2-C(−H). They are marked in purple and green in Figure 5b, respectively. The broad peak at 137 ppm was ascribed to the sp^2-C at the center of GNRs (blue in Figure 5b).

https://dx.doi.org/10.1021/jacs.0c08274
J. Am. Chem. Soc. XXXX, XXX, XXX−XXX

We also measured the impedance spectrum of PIP-DPB (Figure 6). An equivalent circuit shown in the inset of Figure 6

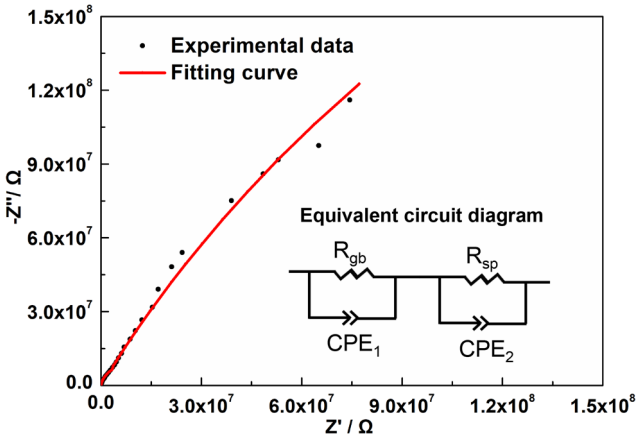

Figure 6. Impedance spectrum of PIP-DPB in Nyquist plot. The equivalent circuit used for fitting is shown.

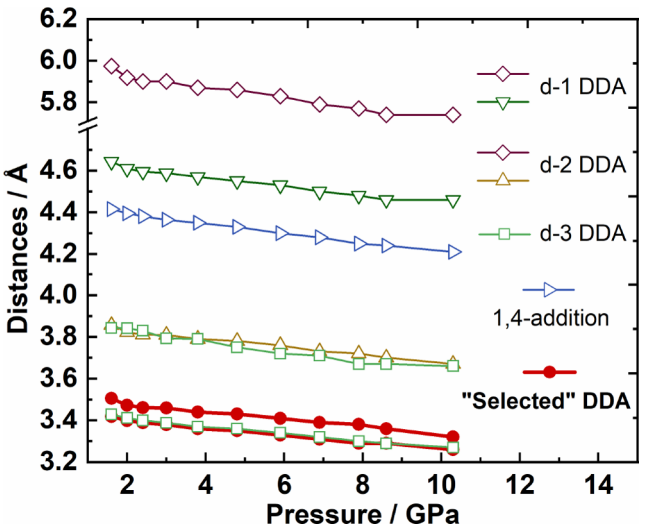

Figure 7. Evolution of the distances mentioned in Scheme 1 during the compression.

was used to fit the Nyquist plot. Considering the electrode area and the thickness of the sample, the permittivities of two semicircles are obtained as about 2.6×10^{-10} and 2.5×10^{-11} F·cm^{-1}, which are recognized as the response from the grain boundary and the second phase, respectively.[36,37] The corresponding resistivities are 7.3×10^7 Ω·cm (grain boundary) and 2.2×10^6 Ω·cm (second phase). Obviously, the polymerization enhanced the conductivity of DPB, which is an insulator. This is due to the formation of conjugated C═C bonds. On the other hand, the resistivity is still higher than that of the conductor, which is probably due to the large proportion of sp^3-carbon in the sample.

Distance-Selected Dehydro-Diels–Alder Reaction of Topochemical Reaction under High Pressure. From the earlier-discussed investigations, we conclude that the DPB undergoes a DDA reaction between the phenyl and phenylethynyl under high pressure and room temperature. The external pressure drives the molecule to reach a certain geometric requirement of SSTP to induce this DDA reaction. The orientation and distance between the reactive carbon atoms are the keys to control the reaction selectivity. As is widely known, for the 1,4-addition SSTP, the geometric requirement is $R_{1,4'} < 4$ Å and $\varphi \approx 45°$, as shown in Scheme 1c, and thermal or photo activation is needed. For the SSTP driven by external pressure, many alkynes react at a critical distance around 3.0 Å at room temperature. For example, acetylene reacts at $d_{C\cdots C} = 3.1$ Å,[28] NaCCH reacts at 2.9 Å,[38] and CaC_2 reacts at 2.8–2.9 Å.[39] Here, for DPB at reaction pressure, the separation of the 1,4′ carbon is ∼4.29 Å (D_3 in Figure 2c), which is larger than the required distance for the 1,4-addition reaction (4 Å) and the empirical distance for a high-pressure reaction (3.0 Å), and hence it inhibits this reaction route. For the DDA reaction, we also found several possible routes as shown in Scheme 1a and d. The evolutions of the mentioned distances in Scheme 1a, c, and d during the compression are plotted in Figure 7, and the distances decrease gradually upon compression. At the critical reaction pressure (10 GPa), the distances between the phenylethynyl and phenyl groups shown in Scheme 1a (∼3.2 Å, D_1 and D_2) are much shorter than the intermolecular C···C distances in the other reaction routes. Hence, this route is preferred as evidenced by our experimental investigations. This is concluded as distance-selectivity in SSTP. The key reason for such a selectivity is that the lattice and the applied pressure restrains the movement of the molecules, so bonding to a remote atom is not favored. Additionally, the distances of 3.2 Å (D_1 and D_2) are similar to that of acetylene under high pressure but much larger than that of benzene.[40,41] This implies that 3.1 Å is the threshold for initiating the reaction of alkyne, regardless of the group with which it is going to react.

Compared to the thermal-/photo-induced SSTP, the external pressure can modify the crystal structure in a vast range and initiate the reaction. What changed is the ground state instead of the vibrational and electronic states in the thermal-/photo-induced SSTP. This also reminds us that these three activation methods can be combined to improve the selectivity and decrease the required pressure, temperature, photon flux, etc.

CONCLUSION

In summary, we explored the SSTP process of DPB under high pressure and room temperature systematically and found that the DPB undergoes a new intermolecular DDA reaction with phenylethynyl as the diene component and phenyl as the dienophile. The geometric configuration for this DDA reaction is determined by in situ high-pressure neutron diffraction. The possibility for other DDA routes and the 1,4-addition reaction are discussed, and the distance-selectivities for these reaction routes are concluded. This reaction produces crystalline GNR with sp^3-carbons at the edge, which may convert to sp^2-carbons by losing hydrogen and will produce a well-defined GNR structure with a clear armchair edge and width of ∼1 nm. Our research highlights that high pressure is an effective tool to overcome the geometry limitation of the molecules and hence drive special distance-selective reactions. Our work also provides a new and designable solid-state synthesis method for bulk crystalline GNRs with atom-scale ordering and controlled width.

https://dx.doi.org/10.1021/jacs.0c08274
J. Am. Chem. Soc. XXXX, XXX, XXX–XXX

■ ASSOCIATED CONTENT

Supporting Information

The Supporting Information is available free of charge at https://pubs.acs.org/doi/10.1021/jacs.0c08274.

Experimental procedures; characterization methods of in situ high-pressure Raman, IR, X-ray diffraction, and neutron diffraction experiments and the impedance of the PIP-DPB experiment; synthetic method of deuterated DPB; characterization of the sample PE-15-washed by X-ray diffraction, scanning electron microscope, high-resolution transmission electron microscope, selected area electron diffraction, neutron pair distribution function measurements, and ^{13}C cross-polarization ($^{1}H-^{13}C$) magic-angle spinning solid-state nuclear magnetic resonance; construction of the structural models of graphitic nanoribbons (GNR-1 and GNR-2); optimization of the crystal structure at 10 GPa; and density functional theory calculation of the IR and NMR spectra of GNR-1 and GNR-2 (PDF)

Crystal structure of DPB optimized by DFT calculation based on the experimental result under 10 GPa (CIF)

Structure model of GNR-1 (CIF)

■ AUTHOR INFORMATION

Corresponding Authors

Kuo Li − *Center for High Pressure Science and Technology Advanced Research, Beijing 100094, P. R. China;* orcid.org/0000-0002-4859-6099; Email: likuo@hpstar.ac.cn

Jing Ju − *College of Chemistry and Molecular Engineering, Peking University, Beijing 100871, P. R. China*; Email: jingju@pku.edu.cn

Authors

Peijie Zhang − *Center for High Pressure Science and Technology Advanced Research, Beijing 100094, P. R. China;* orcid.org/0000-0001-6355-5482

Xingyu Tang − *Center for High Pressure Science and Technology Advanced Research, Beijing 100094, P. R. China*

Yida Wang − *Center for High Pressure Science and Technology Advanced Research, Beijing 100094, P. R. China*

Xuan Wang − *Center for High Pressure Science and Technology Advanced Research, Beijing 100094, P. R. China*

Dexiang Gao − *Center for High Pressure Science and Technology Advanced Research, Beijing 100094, P. R. China*

Yapei Li − *Center for High Pressure Science and Technology Advanced Research, Beijing 100094, P. R. China*

Haiyan Zheng − *Center for High Pressure Science and Technology Advanced Research, Beijing 100094, P. R. China;* orcid.org/0000-0002-4727-5912

Yajie Wang − *Center for High Pressure Science and Technology Advanced Research, Beijing 100094, P. R. China*

Xinxin Wang − *Center for High Pressure Science and Technology Advanced Research, Beijing 100094, P. R. China*

Riqiang Fu − *National High Magnetic Field Laboratory, Tallahassee, Florida 32310, United States;* orcid.org/0000-0003-0075-0410

Mingxue Tang − *Center for High Pressure Science and Technology Advanced Research, Beijing 100094, P. R. China*

Kazutaka Ikeda − *Institute of Materials Structure Science, High Energy Accelerator, Research Organization (KEK), Tsukuba, Ibaraki 305-0801, Japan*

Ping Miao − *Institute of Materials Structure Science, High Energy Accelerator Research Organization (KEK), Tokai, Ibaraki 319-1106, Japan; Institute of High Energy Physics, Chinese Academy of Sciences, Beijing 100049, P. R. China; Spallation Neutron Source Science Center, Dongguan 523803, P. R. China;* orcid.org/0000-0003-1937-1736

Takanori Hattori − *J-PARC Center, Japan Atomic Energy Agency, Tokai, Ibaraki 319-1195, Japan*

Asami Sano-Furukawa − *J-PARC Center, Japan Atomic Energy Agency, Tokai, Ibaraki 319-1195, Japan*

Christopher A. Tulk − *Neutron Scattering Division, Neutron Sciences Directorate, Oak Ridge National Laboratory, Oak Ridge, Tennessee 37830, United States*

Jamie J. Molaison − *Neutron Scattering Division, Neutron Sciences Directorate, Oak Ridge National Laboratory, Oak Ridge, Tennessee 37830, United States*

Xiao Dong − *Key Laboratory of Weak-Light Nonlinear Photonics, School of Physics, Nankai University, Tianjin 300071, P. R. China*

Ho-kwang Mao − *Center for High Pressure Science and Technology Advanced Research, Beijing 100094, P. R. China*

Complete contact information is available at: https://pubs.acs.org/10.1021/jacs.0c08274

Notes

The authors declare no competing financial interest.

■ ACKNOWLEDGMENTS

The authors acknowledge the support of the National Natural Science Foundation of China (NSFC) (Grant nos. 21771011 and 21875006). The authors also acknowledge the support of the National Key Research and Development Program of China (2019YFA0708502). This research used resources of the Advanced Light Source, which is a U.S. Department of Energy (DOE) Office of Science User Facility under Contract no. DE-AC02-05CH11231. This research used resources at the Spallation Neutron Source, a DOE Office of Science User Facility operated by the Oak Ridge National Laboratory. Neutron diffraction experiments at J-PARC were performed through the J-PARC user programs (nos. 2018B0249 and 2018BF2106). High-resolution solid-state ^{13}C NMR were measured at National High Magnetic Field Laboratory supported by the U.S. NSF Cooperative Agreement DMR-1644779 and the State of Florida. The calculations were performed on the TianheII supercomputer at the Chinese National Supercomputer Center in Guangzhou. The authors thank Dr. Haijun Yang for his help in the synthesis of deuterated DPB, Dr. Xiaohuan Lin for her help in the analysis of XRD data, Dr. Xiaoge Wang and Ms. Yunling Jia for their help in the HRTEM experiments, and Dr. Hyun Hwi Lee for his help in the in situ XRD measurements performed in the 5A XRS-MS beamline at the Pohang Accelerator Laboratory (PAL). Dr. K. Li thanks Dr. T. A. Strobel for helpful discussion.

■ REFERENCES

(1) Wegner, G. Topochemical polymerization of monomers with conjugated triple bonds. *Makromol. Chem.* **1972**, *154* (1), 35−48.

(2) Thomas, J. M. Topography and topology in solid-state chemistry. *Philos. Trans. R. Soc., A* **1974**, *277*, 251−286.

(3) Dou, L.; Zheng, Y.; Shen, X.; Wu, G.; Fields, K.; Hsu, W.-C.; Zhou, H.; Yang, Y.; Wudl, F. Single-crystal linear polymers through

visible light-triggered topochemical quantitative polymerization. *Science* **2014**, *343* (6168), 272−277.
(4) Biradha, K.; Santra, R. Crystal engineering of topochemical solid state reactions. *Chem. Soc. Rev.* **2013**, *42* (3), 950−967.
(5) Bloor, D. Topochemical Polymerization: Diynes. In *Comprehensive Polymer Science and Supplements*; Allen, G., Bevington, J. C., Ed.; Elsevier: London, 1989; Vol. *15*, pp 233−249.
(6) Sun, A.; Lauher, J. W.; Goroff, N. S. Preparation of poly(diiododiacetylene), an ordered conjugated polymer of carbon and iodine. *Science* **2006**, *312* (5776), 1030−1034.
(7) Wilhelm, C.; Boyd, S. A.; Chawda, S.; Fowler, F. W.; Goroff, N. S.; Halada, G. P.; Grey, C. P.; Lauher, J. W.; Luo, L.; Martin, C. D.; Parise, J. B.; Tarabrella, C.; Webb, J. A. Pressure-induced polymerization of diiodobutadiyne in assembled cocrystals. *J. Am. Chem. Soc.* **2008**, *130* (13), 4415−4420.
(8) Lauher, J. W.; Fowler, F. W.; Goroff, N. S. Single-crystal-to-single-crystal topochemical polymerizations by design. *Acc. Chem. Res.* **2008**, *41* (9), 1215−1229.
(9) Enkelmann, V. Structural aspects of the topochemical polymerization of diacetylene. *Adv. Polym. Sci.* **1984**, *63*, 91−136.
(10) Baughman, R. H. Solid-state polymerization of diacetylenes. *J. Appl. Phys.* **1972**, *43* (11), 4362−4378.
(11) Jordan, R. S.; Wang, Y.; McCurdy, R. D.; Yeung, M. T.; Marsh, K. L.; Khan, S. I.; Kaner, R. B.; Rubin, Y. Synthesis of graphene nanoribbons via the topochemical polymerization and subsequent aromatization of a diacetylene precursor. *Chem.* **2016**, *1* (1), 78−90.
(12) Enkelmann, V. Solid-state reactivity of triacetylenes. *Chem. Mater.* **1994**, *6* (8), 1337−1340.
(13) Matsumoto, A. Stereospecific polymerization of 1,3-diene monomers in the crystalline state. *Prog. React. Kinet. Mech.* **2001**, *26* (1), 59−110.
(14) Hoang, T.; Lauher, J. W.; Fowler, F. W. The topochemical 1,6-polymerization of a triene. *J. Am. Chem. Soc.* **2002**, *124* (36), 10656−10657.
(15) Johnston, P.; Braybrook, C.; Saito, K. Topochemical photoreversible polymerization of a bioinspired monomer and its recovery and repolymerization after photo-depolymerization. *Chem. Sci.* **2012**, *3* (7), 2301−2306.
(16) Wessig, P.; Müller, G. The dehydro-Diels-Alder reaction. *Chem. Rev.* **2008**, *108* (6), 2051−2063.
(17) Shibata, T.; Sekine, A.; Mitake, A.; Kanyiva, K. S. Intramolecular consecutive dehydro-Diels-Alder reaction for the catalytic and enantioselective construction of axial chirality. *Angew. Chem., Int. Ed.* **2018**, *57* (48), 15862−15865.
(18) Kocsis, L. S.; Brummond, K. M. Intramolecular dehydro-Diels-Alder reaction affords selective entry to arylnaphthalene or aryldihydronaphthalene lignans. *Org. Lett.* **2014**, *16* (16), 4158−4161.
(19) Rodríguez, D.; Navarro-Vázquez, A.; Castedo, L.; Domínguez, D.; Saá, C. Strained intermediates in intramolecular dehydro Diels-Alder reactions: rearrangement of cyclic allenes via 1,2-dehydro[10]-annulenes. *J. Am. Chem. Soc.* **2001**, *123* (37), 9178−9179.
(20) Hoye, T. R.; Baire, B.; Niu, D.; Willoughby, P. H.; Woods, B. P. The hexadehydro-Diels-Alder reaction. *Nature* **2012**, *490* (7419), 208−212.
(21) Wang, T.; Naredla, R. R.; Thompson, S. K.; Hoye, T. R. The pentadehydro-Diels-Alder reaction. *Nature* **2016**, *532* (7600), 484−488.
(22) Di Giovannantonio, M.; Keerthi, A.; Urgel, J. I.; Baumgarten, M.; Feng, X.; Ruffieux, P.; Narita, A.; Fasel, R.; Müllen, K. On-surface dehydro-Diels-Alder reaction of dibromobis(phenylethynyl)benzene. *J. Am. Chem. Soc.* **2020**, *142* (4), 1721−1725.
(23) Bini, R.; Ceppatelli, M.; Citroni, M.; Schettino, V. From simple to complex and backwards. Chemical reactions under very high pressure. *Chem. Phys.* **2012**, *398*, 262−268.
(24) Yoo, C.-S. Chemistry under extreme conditions: pressure evolution of chemical bonding and structure in dense solids. *Matter Radiat. at Extremes* **2020**, *5* (1), 018202.
(25) Zhao, D.; Wang, M.; Xiao, G.; Zou, B. Thinking about the development of high-pressure experimental chemistry. *J. Phys. Chem. Lett.* **2020**, *11* (17), 7297−7306.
(26) Yang, X.; Wang, X.; Wang, Y.; Li, K.; Zheng, H. From molecules to carbon materials-high pressure induced polymerization and bonding mechanisms of unsaturated compounds. *Crystals* **2019**, *9* (10), 490.
(27) Wang, X.; Li, K.; Zheng, H.; Zhang, P. Chemical reactions of molecules under high pressure. *Chem. Bull.* **2019**, *82* (5), 387−398.
(28) Sun, J.; Dong, X.; Wang, Y.; Li, K.; Zheng, H.; Wang, L.; Cody, G. D.; Tulk, C. A.; Molaison, J. J.; Lin, X.; Meng, Y.; Jin, C.; Mao, H.-k. Pressure-induced polymerization of acetylene: structure-directed stereoselectivity and a possible route to graphane. *Angew. Chem., Int. Ed.* **2017**, *56* (23), 6553−6557.
(29) Tang, W. S.; Strobel, T. A. Pressure-induced solid-state polymerization of optically-tunable diphenyl-substituted diacetylene. *ACS Appl. Polym. Mater.* **2019**, *1* (12), 3286−3294.
(30) Melveger, A. J.; Baughman, R. H. Raman spectral changes during the solid-state polymerization of diacetylenes. *J. Polym. Sci., Polym. Phys.* **1973**, *11* (4), 603−619.
(31) Birch, F. Finite strain isotherm and velocities for single-crystal and polycrystalline NaCl at high pressures and 300 ∘K. *J. Geophys. Res.: Solid Earth* **1978**, *83* (B3), 1257−1268.
(32) Jordan, R. S.; Li, Y. L.; Lin, C.-W.; McCurdy, R. D.; Lin, J. B.; Brosmer, J. L.; Marsh, K. L.; Khan, S. I.; Houk, K. N.; Kaner, R. B.; Rubin, Y. Synthesis of N = 8 armchair graphene nanoribbons from four distinct polydiacetylenes. *J. Am. Chem. Soc.* **2017**, *139* (44), 15878−15890.
(33) Hopf, H.; Musso, H. Preparation of benzene by pyrolysis of cis- and trans-l,3-hexadien-5-yne. *Angew. Chem., Int. Ed. Engl.* **1969**, *8* (9), 680.
(34) Prall, M.; Krüger, A.; Schreiner, P. R.; Hopf, H. The cyclization of parent and cyclic hexa-1,3-dien-5-ynes-a combined theoretical and experimental study. *Chem. - Eur. J.* **2001**, *7* (20), 4386−4394.
(35) Lu, T.; Chen, F. Multiwfn: a multifunctional wavefunction analyzer. *J. Comput. Chem.* **2012**, *33* (5), 580−592.
(36) Sinclair, D. C. Characterization of electro-materials using ac impedance spectroscopy. *Bol. Soc. Esp. Cerám. Vidrio* **1995**, *34* (2), 55−65.
(37) Irvine, J. T. S.; Sinclair, D. C.; West, A. R. Electroceramics: characterization by impedance spectroscopy. *Adv. Mater.* **1990**, *2* (3), 132−138.
(38) Han, J.; Tang, X.; Wang, Y.; Wang, Y.; Han, Y.; Lin, X.; Dong, X.; Lee, H. H.; Zheng, H.; Li, K.; Mao, H.-k. Pressure-induced polymerization of monosodium acetylide: a radical reaction initiated topochemically. *J. Phys. Chem. C* **2019**, *123* (50), 30746−30753.
(39) Zheng, H.; Wang, L.; Li, K.; Yang, Y.; Wang, Y.; Wu, J.; Dong, X.; Wang, C.-H.; Tulk, C. A.; Molaison, J. J.; Ivanov, I. N.; Feygenson, M.; Yang, W.; Guthrie, M.; Zhao, Y.; Mao, H.-K.; Jin, C. Pressure induced polymerization of acetylide anions in CaC_2 and 10^7 fold enhancement of electrical conductivity. *Chem. Sci.* **2017**, *8* (1), 298−304.
(40) Ciabini, L.; Santoro, M.; Gorelli, F. A.; Bini, R.; Schettino, V.; Raugei, S. Triggering dynamics of the high-pressure benzene amorphization. *Nat. Mater.* **2007**, *6* (1), 39−43.
(41) Wang, Y.; Dong, X.; Tang, X.; Zheng, H.; Li, K.; Lin, X.; Fang, L.; Sun, G.; Chen, X.; Xie, L.; Bull, C. L.; Funnell, N. P.; Hattori, T.; Sano-Furukawa, A.; Chen, J.; Hensley, D. K.; Cody, G. D.; Ren, Y.; Lee, H. H.; Mao, H.-k. Pressure-induced Diels-Alder reactions in C_6H_6-C_6F_6 cocrystal towards graphane structure. *Angew. Chem., Int. Ed.* **2019**, *58* (5), 1468−1473.

https://dx.doi.org/10.1021/jacs.0c08274
J. Am. Chem. Soc. XXXX, XXX, XXX−XXX